Integrated Project (IP)
Project No. TIP5-CT-2006-031415

Thematic Priority 6:
Sustainable Development,
Global Change and Ecosystems

Modelling of the track subgrade

Part 1: Final report on the modelling of poor quality sites

Part 2: Variability accounting in numerical modelling of the track subgrade




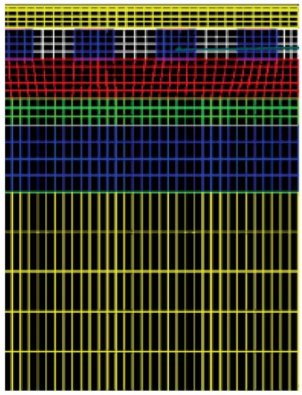

INNOTRACK GUIDELINE

Deliverable D2.1.12

Table of Contents

Part 1: Final report on the modelling of poor quality sites

Part 2: Variability accounting in numerical modelling of the track subgrade

Executive Summary

Part 1 of this guideline is oriented towards physical and numerical modelling of poor quality sites. Presented finite element simulations demonstrate a unifying methodology to design the railway subbase. The approach is easily extensible in such a way, that various reinforcing means can be included.

As variability is not commonly taken into consideration in numerical simulations, the aim of part 2 of this guideline is to quantify the uncertainties and variabilities of mechanical properties due to the natural randomness and scattering in subgrade properties. The aim is to demonstrate how to build stochastic models from deterministic ones.

Part 1:

Final report on the modelling of poor quality sites

1. Introduction

In order to develop a new method for design of the railway substructure using a multilayer approach, a set of Finite Element Models have been developed. To evaluate the possibilities of the models to reflect behaviour of the real construction, a set of experiments using a test box with different designs of construction layers is used. Bearing capacity of the construction has been assessed and compared to values obtained from numerical simulations.

A series of laboratory measurements on model constructions with poor subgrade in scale 1:1 was carried out. This included both short-term and long-term loading. Obtained data were used as an input for numerical analysis.

The aim of this study is to utilize numerical modelling to develop a set of design graphs for the construction of a railway substructure. The FE models represent load tests of the construction using circular plates. Bearing capacity is calculated from the material response.

The studied models were:

1. plane strain FE model for bearing capacity assessment
2. 3-D FE model of the test box
3. 3-D FE model of the in-situ conditions

The FE model in case 2 featured the test box – a part of the track bed in 1:1 scale in which all the configurations are to be studied. Case 3 is an extension of the results to real track conditions.

In this guideline, bearing capacity assessment using the plane strain FE models (case 1) and resulting nomograms are covered. Details on this study can be found in INNOTRACK reports D2.1.3 and D2.1.16.

2. Physical modelling

2.1. Test box

A series of laboratory measurements on substructure models with dimensions of 2 x 1 x 0.8 m were performed in the test box of Czech Technical University in Prague (Fig. 1). The substructure was modelled in a 1:1 scale. In order to ensure constant characteristics, the subgrade consisted of a layer of rubber with a known bearing capacity (to simulate a poor subgrade, static modulus of deformation was choosen as 20 MPa and 30 MPa).

Fig. 1 Test box

The subgrade was covered by a sub-ballast layer of crushed stone mixture with a constant thickness of 20 cm. A ballast bed with thicknesses of 25 cm, 35 cm and 45 cm was placed on the sub-ballast layer, and a concrete half-sleeper with and without a resilient under-sleeper pad was mounted onto it.

2.2. Loading

All model constructions were loaded with subsequent static loads (in the order of tens of load cycles). Selected model constructions were cyclically loaded with a total number of 250 thousand load cycles.

Short-term loaded model constructions were manually loaded with forces corresponding to axle loads of 22.5 t, 25.0 t and 27.5 t, whilst

long-term loaded model constructions were loaded only with a force corresponding to an axle load of 22.5 t.

The load exerted onto the sleeper by the axle force was calculated from a model of a beam resting on resilient supports. The calculation assumed a UIC 60 rail, a B91 S/1 sleeper, and a sleeper distance of 0.6 m.

The cyclic loading of the substructure was performed with a powerful hydraulic load cylinder (Fig. 2) mounted on a rigid steel frame. The load apparatus was operated by means of a special control and recording unit.

Fig. 2 Hydraulic load cylinder

Under cyclic loading, the rail head was loaded with a force ranging from 2 to 42 kN with a sinusoidal pattern and a frequency of 3 Hz. The model constructions loaded by 250 000 cycles had settlements of monitored points determined before loading and after 100, 1 000, 10 000, 50 000, 100 000 and 250 000 cycles.

2.3. Monitored parameters

The settlements of superstructure and substructure were monitored during the loading process (Fig. 3), and the bearing capacity of the

individual substructure layers was successively determined by means of a static plate load test (Fig. 4) and an impact load test. In addition, a series of supplementary laboratory tests were carried out to determine additional parameters (e.g. volume density, homogeneity of layers).

Fig. 3 Measurement of settlement under short-term loading

Fig. 4 Static plate load test

2.4. Results

While increasing axle loads from 22.5 t to 25.0 t or 27.5 t measured data imply that on models with sleeper that lack under-sleeper pads,

the increased elastic sleeper settlement is lower than the relative increase in load magnitude. Another finding is that on models with a sleeper eqquiped with an under-sleeper pad, the elastic sleeper settlement can be, depending on type of under-sleeper pad, more than 5 times greater than for models without the under-sleeper pad. In this case, the increased settlement due to a higher axle-load was significantly lower.

The modulus of deformation on the ballast surface in models with a sleeper without a resilient under-sleeper pad as well as in models with a resilient under-sleeper pad grows in a similar way with the ballast layer. In constructions with ballast thickness of 45 cm, the modulus of deformation determined on the ballast surface was roughly twice the value determined on constructions with a ballast thickness of 25 cm.

The permanent settlement of a half-sleeper, i.e. the settlement of the ballast layer, was in the model with ballast thickness 25 cm and subgrade load-bearing capacity of 30 MPa after 250 000 loading cycles decreased by more than 55 % by using under-sleeper pad (Fig. 5).

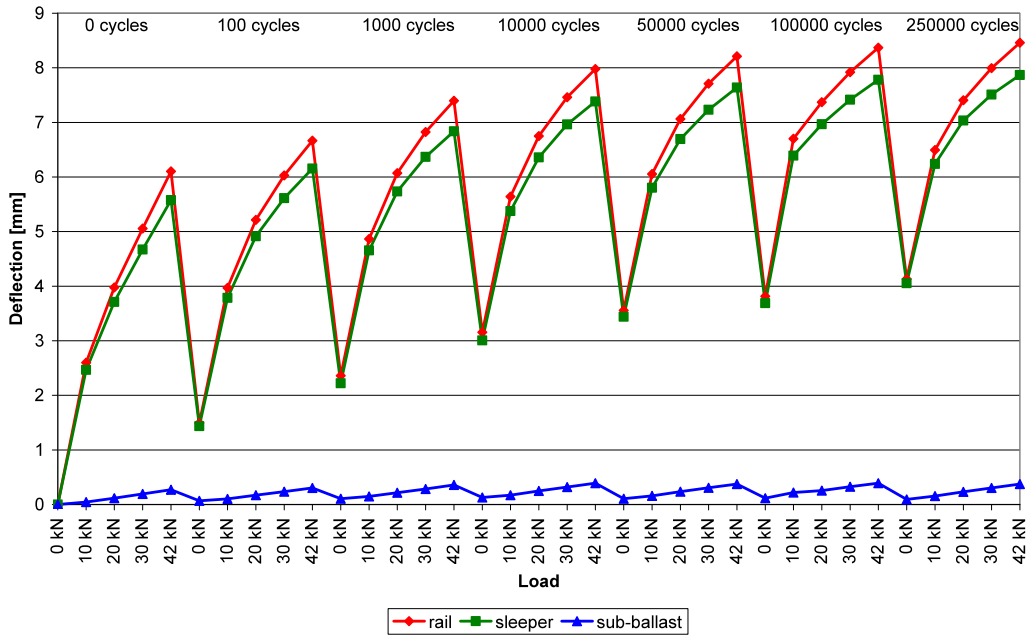

Fig. 5 Settlement of a model with under-sleeper pad (example)

3. FE modelling verification against laboratory experiments

To verify the FE modelling approach a detailed 3-D FE model of the test box was developed and loaded according to the experiments. Three load cases were considered for each test configuration a axle load according to 22.5 t, 25.0 t and 27.5 t.

3.1. Description of the FE models

The laboratory set-up is considered as a three dimensional elasticity contact problem, where no symmetry is employed. The FE model consists of three layers. The bottom layer represents the rubber plate. On top of the rubber plate there are two layers representing the sub-ballast layer and a layer of ballast. The concrete sleeper is placed on the ballast layer with the bottom face covered with contact elements to simulate the interaction with the underlying layer. The model is depicted in Fig.6.

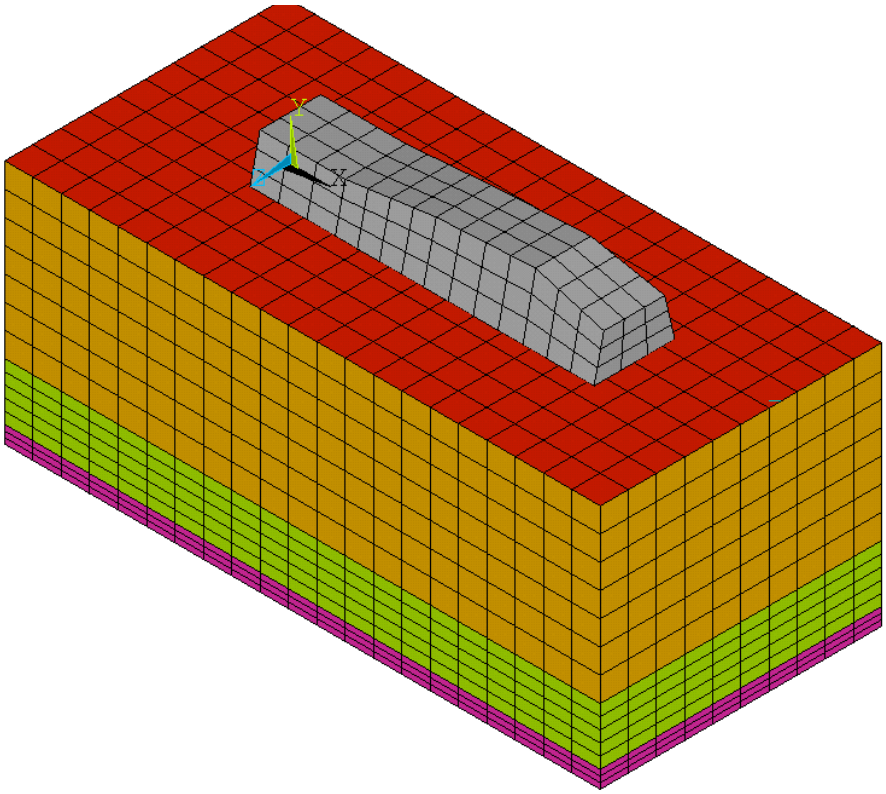

Fig. 6 FE model of the test box

3.2. Finite elements used

The geometry of all layers is discretized using is a 20-node 3-D solid element with quadratic shape functions. In each nodal point three degrees of freedom are defined: translation in the x, y, and z directions.

The contact between the concrete sleeper and the layer of gravel is considered as a frictional and modelled using higher-order contact elements. Coulomb friction is defined with coefficient of friction 0.6.

3.3. Material properties

The magnitude of the stresses in considered materials motivates a presumption of linear elastic material properties for all layers. Material properties assigned to the materials are:

Material	Young's modulus of elasticity E [MPa]	Poisson's ratio μ [-]
concrete sleeper	23 000	0.23
ballast	80	0.23
sub-ballast	60	0.26
rubber layer	2-10	0.45

Tab. 1: Material properties employed in the FE model

3.4. Loading

The model is loaded according to the experiments. The top surface of the concrete sleeper is loaded with a load corresponding to an axle load of 22.5 t, 25.0 t and 27.5 t. For each load case and for each configuration considered (different thickness of ballast the layer - 25 cm, 35 cm and 45 cm) the vertical displacements are computed at locations where settlements were measured. An example of the stress distribution is presented in Fig.7**Error! Reference source not found.**.

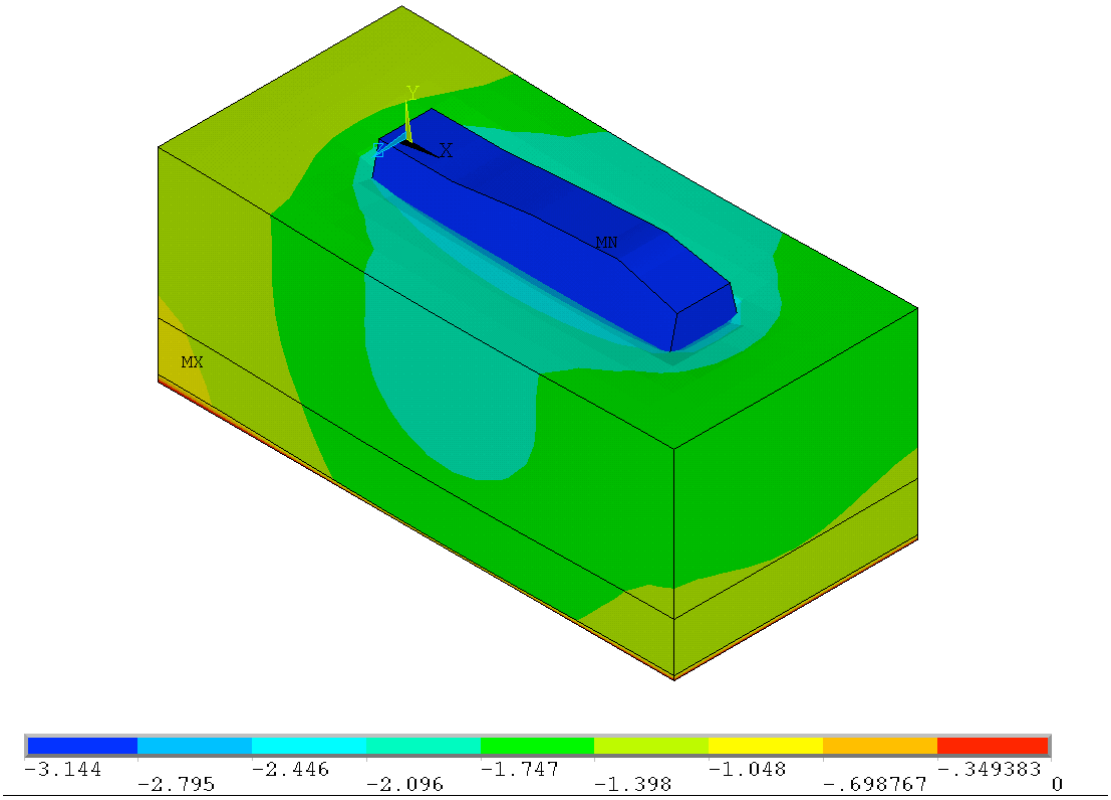

Fig. 7 Example of 3rd principal stress distribution evaluated in the FE simulation

The results from the FE analysis show good correspondence with expected results and with the settlements measured experimentally, see Tab. 2. Further, the strains in the rubber layer were compared with strain gauge measurements and showed good agreement.

After the verification of the FE models of the test box the model was used to derive the relationship between the thickness of the construction layers and resulting bearing capacity of the construction. This enables the establishment of design graphs for different configurations of the sub-base.

Deflection Meter	Experimental [mm]	Num. Model [mm]	deviation [-]
1	0.63	0.8016	0.11
2	0.67	0.8016	
3	0.77	0.8050	
4	0.79	0.8050	
average	**0.72**	**0.8**	
A	0.30	0.4072	0.18
B	0.36	0.4072	
C	0.32	0.3792	
D	0.33	0.3792	
average	**0.33**	**0.39**	

Tab. 2 Vertical displacements at places of deflection meters for applied load 22.5 tons of model with 45 cm thick ballast

4. Desing graphs for single layer construction

The bearing capacity of a single layer construction is evaluated using circular plate (radius 150 mm) with an applied pressure (p=0.2 MPa). The thickness of the sub-ballast layer is varied to find the required modulus of deformation for the entire construction.

No	Young's modulus calculation	Remarks
1	Values of the Young's modulus can be calculated from the oedometric modulii of deformation and Poisson's ratio for the case of plain strain given by boundary conditions $\varepsilon_z = 0$. The equation describing compression of soil is simply written as: Where is oedometrical modulus, is the stress in z-direction, is strain in z-direction and is the vertical deflection.	
2	The relation between and Young's modulus of elasticity is derived from the extended Hook's law. The relationship can be expressed as:	

The results of the numerical analyses were developed into a set of design graphs. With the help of the nomograms and a known stiffness of the subgrade it is easy to find the appropriate thickness of the ballast layer to obtain a given modulus of deformation E_{required}.

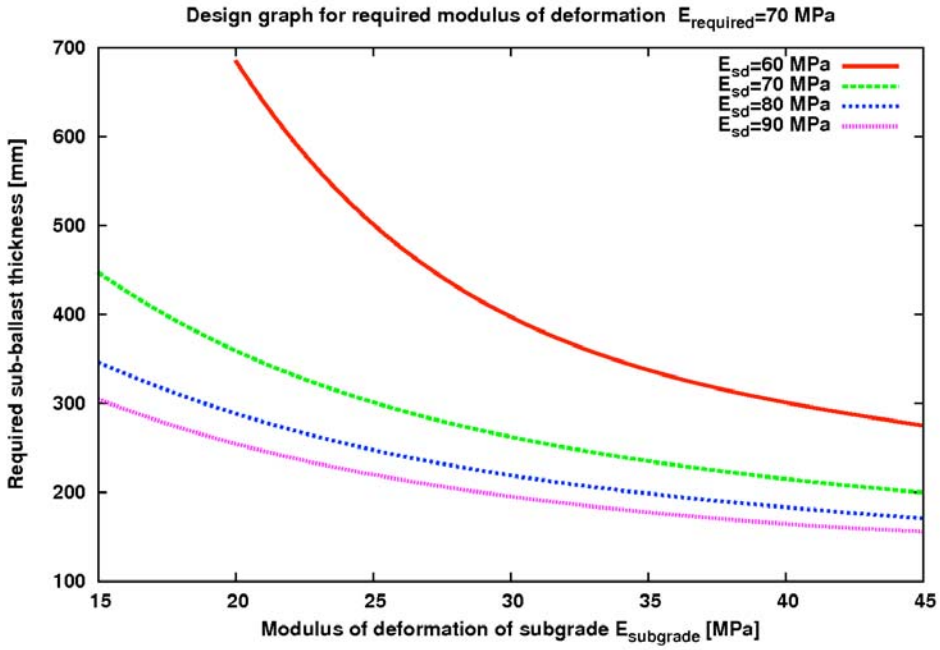

Fig. 8 Design graph for a required modulus of deformation E=70 MPa

Figure 8 shows a design graph for a required modulus of deformation E = 70 MPa. On the horizontal axis the modulus of deformation of the existing subgrade is given and for each modulus of deformation of the ballast a design curve is plotted. Vertical axis lists ballast thickness.

5. Desing graphs for double layer constructions

FE models can be extended to double layer construction where not only the thickness of the ballast and the sub-ballast layer are varied, both. Usage of these design graphs is similar to the single layer construction graphs. For the required modulus of deformation an appropriate construction can be found given the material properties and modulus of deformation of the subgrade and ballast material.

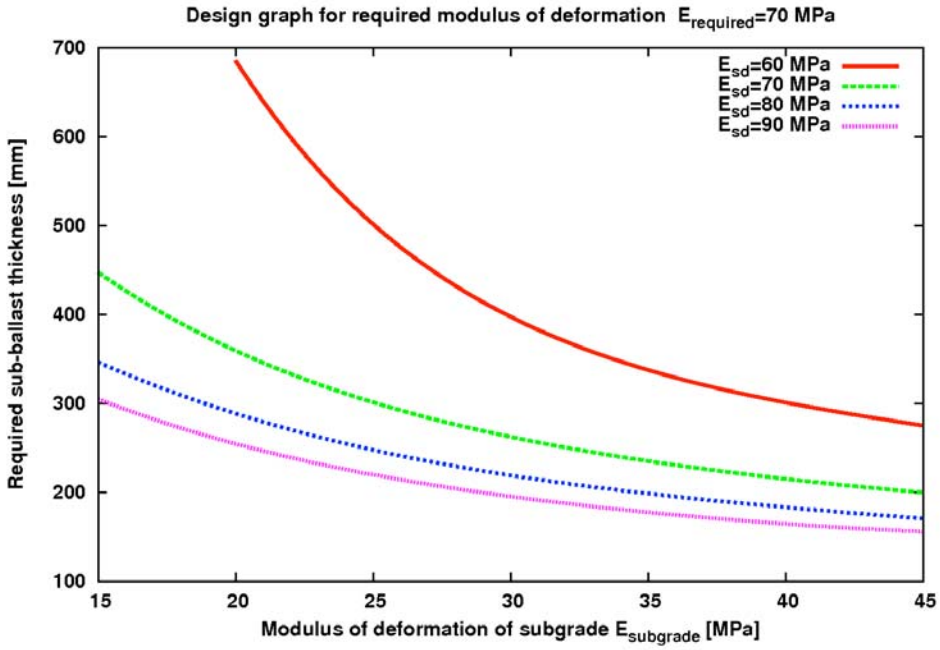

Fig. 9 Design graph for required modulus of deformation E=70 MPa, thickness of the top ballast layer 250 mm

6. Conclusions

The presented finite element models show an unifying methodology to design the railway subbase. The approach is extensible in the sense that reinforcement (e.g. geosynthetics or cement layers) can be included. For each design, bearing capacity can be readily evaluated. This enables an optimal solution to the specific problem given.

Part 2:

Variability accounting in numerical modelling of the track subgrade

7. Introduction

Deterioration of the track geometry is an important contribution to maintenance costs. This deterioration is mainly caused by the settlement of the substructure which tends to depend on site conditions.

To provide a realistic description of the mechanical behaviour of a railway track under dynamic loads, it is necessary to use a numerical model able to account for uncertainties in mechanical and geometrical parameters. Several numerical approaches based on the Finite Element Method (FEM) have been developed in the last decades to describe the global or local behaviour of railway tracks. To take random variability into consideration, the natural extension is to employ a Stochastic Finite Element Method (SFEM).

In the frame of the Innotrack project, this guideline aims at proposing:

- a numerical method,
- an application to railway track problems.

8. Finite Element Modelling of a railway track

A 2D multi-layer finite elements model representing a traditional railway section is developed (Fig. 10). The model is a compromise between accuracy and computations costs.

For the superstructure (rail, sleepers and pads) and the non compacted ballast layer, an elastic linear behaviour is presumed.

Elastic-plastic behaviour with linear strain hardening is chosen for ballast and subgrade layers due to the importance of irreversible stains.

The strain hardening modulus (H) of each component is deduced from the elastic modulus E ($H = \frac{1}{4}E$) in order to minimise the number of parameters.

Normal displacements of lateral and lower boundaries are prohibited. Two vertical loads of magnitude 85 kN and with a separation of 3 m, modelling a train boogie, are applied as traversing at a speed of 160 km/h along the rail.

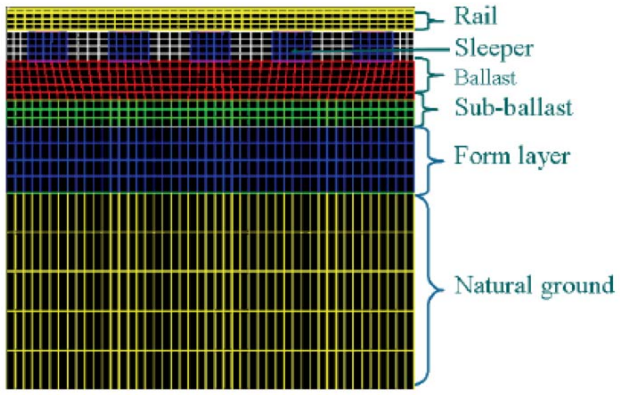

Fig. 10 2D multi-layer finite elements model

In the simulations, Cast3m FE code (Cast3m 2007) has been used. The total length of the developed model was about 30m (50 sleepers). The final mesh consisted in 12792 elements and 13577 nodes (cf. previous figure).

9. Validation of the Track Finite Element Model

The validation was carried out towards deflection and acceleration signals measured in a traditional railway and towards numerical results using Dynavoie 2.0 code.

Fig. 11 shows athe comparison of the vertical acceleration under the 20th sleeper. Results of the FE model are in good agreement with experimental and additional numerical results.

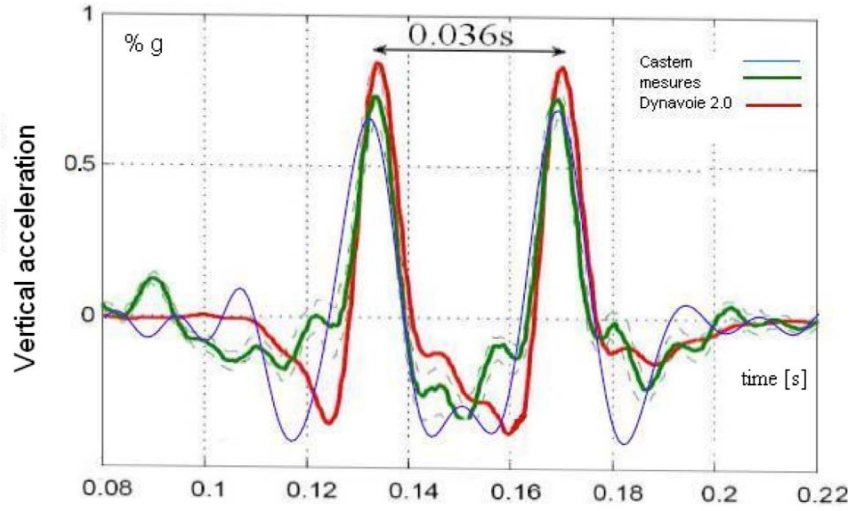

Fig. 11 Comparison of experimental and numerical predictions of the vertical acceleration under the 20th sleeper ($^{\%g}$)

10. Uncertain Parameters

The uncertain parameters of the FE model are, for each of the four layers making up the railway subgrade (ie. Ballast, sub-ballast, form layer, silt layer) presumed to be:

- the thickness
- the Young modulus.

		notation	Mathematical notation	m_{Y_i}	σ_{Y_i}
thickness (m)	Ballast	h_b	Y_1	0.26	0.11
	Sub-ballast	h_{sb}	Y_2	0.64	0.25
	form layer	h_f	Y_3	0.97	0.59
	silt layer	h_l	Y_4	1.62	0.69
Young modulus (MPa)	Ballast	E_b	Y_5	38.91	11.27
	Sub-ballast	E_{sb}	Y_6	26.55	18.27
	form layer	E_f	Y_7	9.21	5.84
	silt layer	E_l	Y_8	10.74	8.61

Tab. 3: The uncertain parameters

The R^8-valued random variables (rv) $Y = (Y_1,...,Y_8)^T$ is the mathematical representation of the uncertain parameters. A statistical analysis from in-situ measurements on a traditional railway track has shown that the coordinates Y_k can be assumed mutually independent and that experimental distribution of each rv Y_k is in good agreement with a Log-normal distribution.

By extension, Y is presumed to be Log-normal with independent components. The mean m_{Y_i} and the standard deviation σ_{Y_i} of each rv Y_i are listed in Tab. 3.

It should be noticed that, due to the nature of the Y_i's (soil characteristics) the coefficients of variation $CV_{Y_i} = \sigma_{Y_i}/m_{Y_i}$ of these rv's are great.

The deterministic parameters are given in the next table.

Component	E (MPa)	ν	Thickness (mm)	ρ (kg/m3)
Non-compacted Ballast	20	0.3	210	1300
Rails	2.10^5	0.3	UIC60 profile	7850
Pads	40	0.25	9	900
Sleepers	3.10^4	0.25	210	2400

Tab. 4: Values of the deterministic parameters

11. Control variables

Four control variables are chosen:

- maximum deflection under the 25^{th} sleeper (centre of the geometrical model) simulated during the period T: S_d
- maximum acceleration under the 25^{th} sleeper: S_a
- maximum rail deflection: R_d
- levelling indicator: NL, defined as the standard deviation of the sample formed by the deflection variation recorded at each computation time between the two boogie axles.

These variables are linked to the displacement field $\mathbf{Q} = (\mathbf{Q}(t), t \in \mathsf{R}_+)$ of the FE model, and more precisely to a scalar or vector observation $\mathbf{Z} = (\mathbf{Z}(t), t \in \mathsf{R}_+)$ of this field.

Since the parameters $Y_1,...,Y_8$ are rv's, $\mathbf{Q}$ and $\mathbf{Z}$ are stochastic processes and consequently the control variables S_d, S_a, R_d and NL are rv's that are denoted:

$$M_1 = S_d\ , \quad M_2 = S_a\ , \quad M_3 = R_d\ , \quad M_4 = NL$$

The proposed SFE method is suited to the calculation of the second order statistics of these rv's.

12. Numerical convergence study

In order to simplify the presentation, only one random parameter (the ballast thickness $Y_1 = h_b$) is considered in the following. The statistics of other parameters, considered as deterministic, are taken equal to their mean values.

Instead of reaching a rigorous numerical convergence, the following tests aim at determining the minimum number of collocation to accurately evaluate the two first statistical moments of the control variables M_i. The number of collocation points is chosen between 2 and 8. At the same time Monte-Carlo Simulations (MCS) for the considered model are carried out. Only 1000 Monte-Carlo realisations are employed for computational reasons (one deterministic FE computation is about 40 minutes).

A convergence of the mean and the standard deviation of control variables according to the MCS number appears for less than 100 simulations. This number of simulations is sufficient for a good estimation of the two first statistical moments but remains insufficient to obtain a good estimation of the probability density. An example of convergence analysis of the mean and the standard deviation of $M_1 = S_d$ as a function of the MCS number is given in Fig. 12.

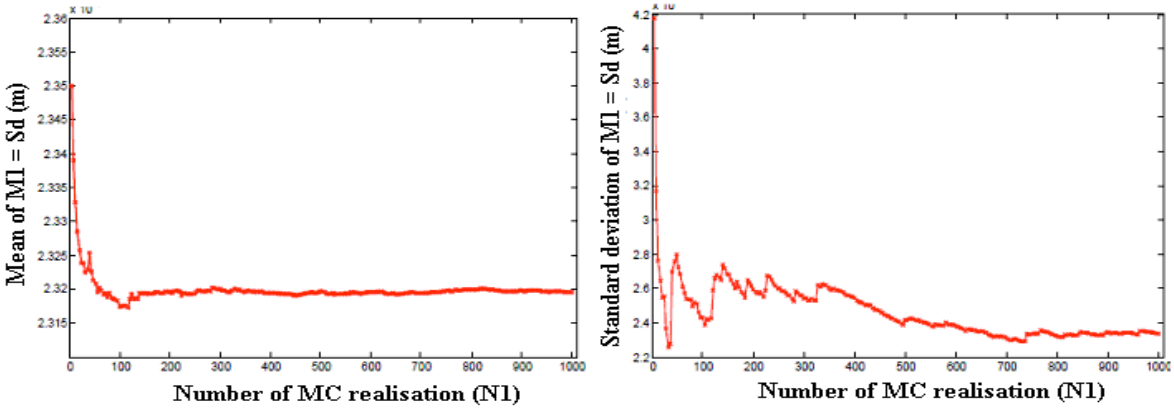

Fig. 12 Evolution of the mean (left) and the standard deviation (right) of $M_1 = S_d$ as a function of the MCS number

The convergence of the mean and the standard deviation of control rv's according to collocation points number is then analyzed and compared to values obtained from MCS.

For instance, the following figures show the evolution of respectively the mean m_{M_1} and the standard deviation σ_{M_1} of the sleeper deflection $M_1 = S_d$ for increasing the number of collocation points and the comparison to the reference value (MCS results).

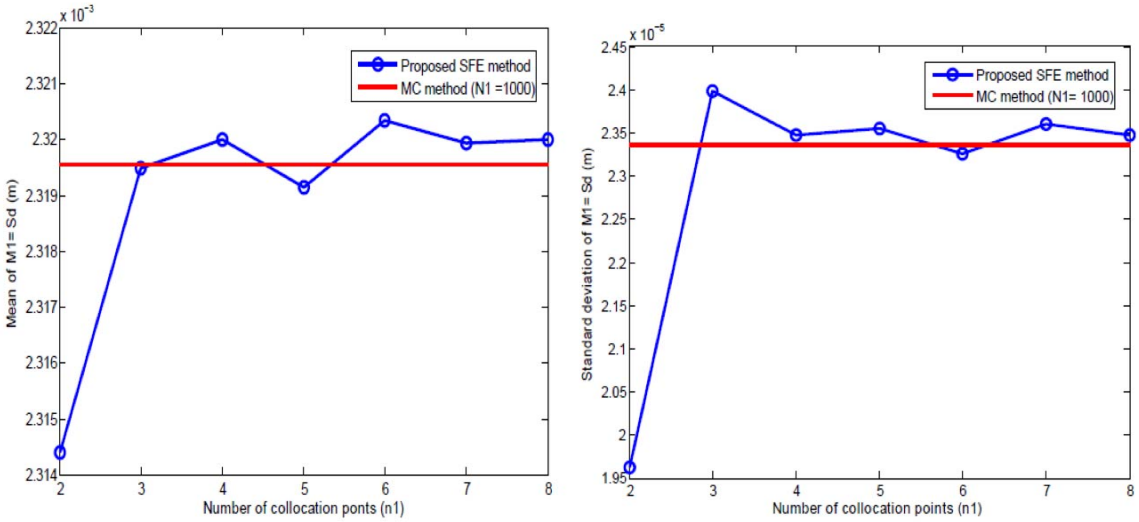

Fig. 13 Evolution of the mean (left) and the standard deviation (right) of $M_1 = S_d$ according to the number of collocation points

From Fig. 13, convergence of mean and standard deviation of the selected random parameters is achieved. The same remarks can be drawn from the other output parameters.

A good compromise between computational effort and precision corresponds to 4 collocation points.

In Tab. 5, results from studies with 4 collocation points and MCS including all simulations are given. Results show that the mean and the standard deviation of the different control parameters are of the same magnitude.

	CM (4 points)		MCS (1000)	
	m_{M_i}	σ_{M_i}	m_{M_i}	σ_{M_i}
$NL\ (10^{-4} m)$	2.26	0.114	2.25	0.112
$R_d\ (10^{-3}\ \mathrm{m})$	2.58	0.0378	2.58	0.0443
$S_d\ (10^{-3}\ \mathrm{m})$	2.32	0.0257	2.32	0.0238
$S_a\ (\mathrm{m/s}^{-2})$	6.69	1.69	6.66	1.17

Tab. 5: Mean and standard deviation of (^{M_i}) obtained with collocation method (CM) and Monte-Carlo Simulations (MCS)

13. Numerical railway applications

The results of successive parametric studies meant to quantify the uncertainty propagation through the proposed numerical model are presented in this section.

For each study, only one random parameter Y_i is considered and its distribution is assumed to be Lognormal with given mean m_{Y_i} and coefficient of variation $CV_{Y_i} = \sigma_{Y_i}/m_{Y_i}$.

The uncertainty propagation analysis is carried out with three values of CV_{Y_i} for each Y_i: the experimental value $CV_{Y_i}^{exp}$ obtained from Tab. 3 and 80 % and 120 % of $CV_{Y_i}^{exp}$.

This analysis consists in quantifying the influence of the random variability of each Y_i on the random variability of the control variables M_i, the coefficients of variation being used to express these random variables.

As an illustration, Fig. 14 shows the evolution of the coefficient of variation CV_{M_1} of the control variable $M_1 = S_d$ according to the coefficient of variation CV_{Y_i} of each random parameter Y_i.

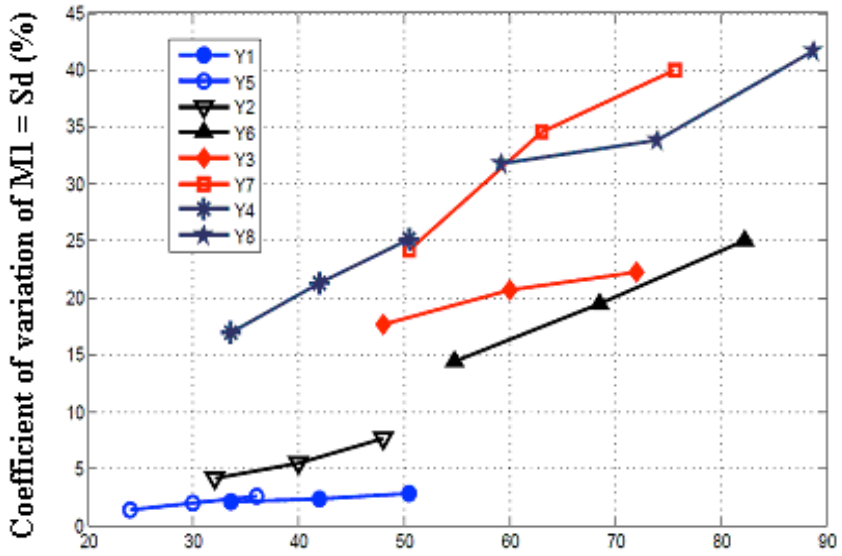

Y_1	h_b
Y_2	h_{sb}
Y_3	h_f
Y_4	h_l
Y_5	E_b
Y_6	E_{sb}
Y_7	E_f
Y_8	E_l

Fig. 14 Evolution of the coefficient of variation of $M_1 = S_d$ according to the coefficient of variation of each random parameter Y_i

In order to clearly illustrate the influence of each random parameter Y_i on the scattering of the control rv. $M_1 = S_d$, the increase ΔCV_{M_1} in CV_{M_1} (corresponding to the increase $\Delta CV_{Y_i} = 1.2CV_{Y_i}^{exp} - 0.8CV_{Y_i}^{exp} = 0.4CV_{Y_i}^{exp}$ in CV_{Y_i}) is estimated for each Y_i.

The obtained results are listed in the following table. They show that the most influential parameter is the Young modulus of the form-layer $Y_7 = E_f$. The parameters $Y_4 = h_l$ and $Y_8 = E_l$ have also an important influence. But the thickness of the silt layer h_l is difficult to estimate from in-situ measurements due to limitations of the test depths.

Tab. 6 also shows that the random parameters $Y_1 = h_b$ and $Y_5 = E_b$ have a small influence on the scattering of $M_1 = S_d$.

	Y_1	Y_5	Y_2	Y_6	Y_3	Y_7	Y_4	Y_8
	h_b	E_b	h_{sb}	E_{sb}	h_f	E_f	h_l	E_l
ΔCV_{M_1}	1.6	2.9	7.0	9.4	7.9	21.6	12.3	11.8

Tab. 6: Values of ΔCV_{M_1} corresponding to $0.4CV_{Y_i}^{exp}$ for each random parameter

All the obtained results in the study are summarized in the Fig. 15. In this figure ΔCV_{M_j}'s of all the control rv M_j's for each random parameter Y_i are given.

It can be seen that the Young modulus of form-layer ($Y_7 = E_f$) and of the sub-ballast ($Y_6 = E_{sb}$) have a major influence on the variability of most random parameters and particularly on the sleeper deflection $M_1 = S_d$ and the leveling indicator $M_4 = NL$.

More generally, the influence of the variability of the mechanical parameters (Young's modulus $Y_5 = E_b$, $Y_6 = E_{sb}$, $Y_7 = E_f$, $Y_8 = E_l$) is more significant than the corresponding thicknesses $Y_1 = h_b$, $Y_2 = h_{sb}$, $Y_3 = h_f$, $Y_4 = h_l$.

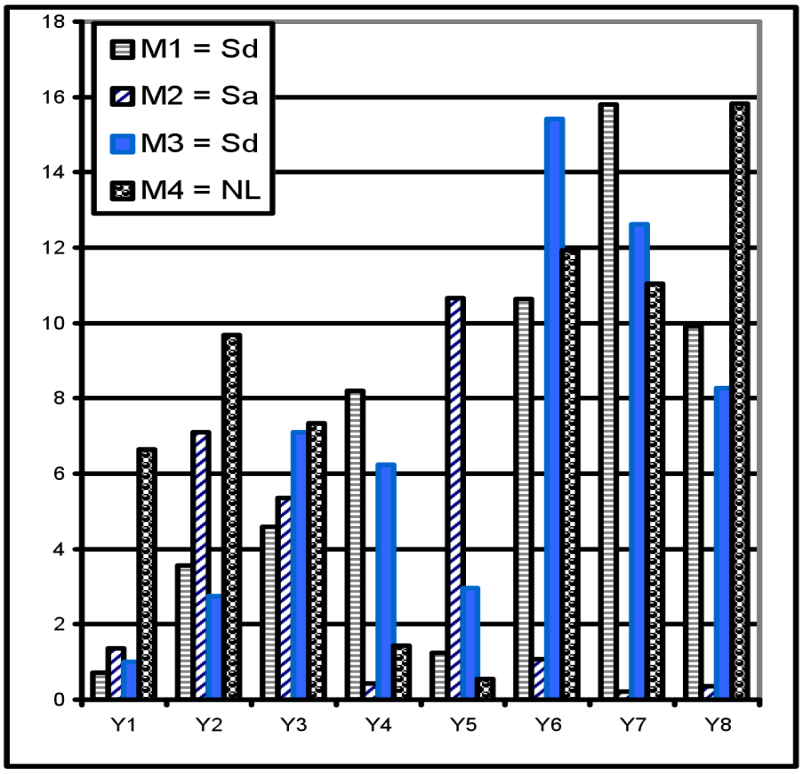

Y_1	h_b
Y_2	h_{sb}
Y_3	h_f
Y_4	h_l
Y_5	E_b
Y_6	E_{sb}
Y_7	E_f
Y_8	E_l

Fig. 15 ΔCV_{M_j} for every random parameter Y_i

Another way to analyse the influence of the parameter's variability is to use uncertainty propagation factors, which are positive coefficients associated with each control variable M_i. The uncertainty propagation factor relative to the control variable M_i is defined, $\forall k \in \{1,...,8\}$:

$$\alpha_i(k) = \frac{\Delta CV_{M_i}(k)}{\sum_{j=1}^{8} \Delta CV_{M_i}(j)}, i = 1,...,4$$

where $\Delta CV_{M_i}(j)$ is the increase of the M_i coefficient of variation associated with the increase of the Y_j coefficient of variation. For a given control rv, the random parameter corresponding to the largest value of this factor is thus the parameter having the largest influence.

Fig. 16 shows a graphic repartition of such a factor for all the random parameters. It highlights the major influence of the form-layer Young modulus $Y_7 = E_f$ on three of the four control variables.

For the levelling indicator $M_4 = NL$ and the rail deflection $M_1 = S_d$, the parameters $Y_4 = h_l$, $Y_6 = E_{sb}$ and $Y_7 = E_f$ are the most influential random parameters while the ballast parameters $Y_1 = h_b$ and $Y_5 = E_b$ have a small influence. The sleeper acceleration $M_2 = S_a$ is more sensitive to $Y_1 = h_b$ and $Y_5 = E_b$, and the Young modulus of the silt layer $Y_4 = E_l$ has a small influence on most of the control variables.

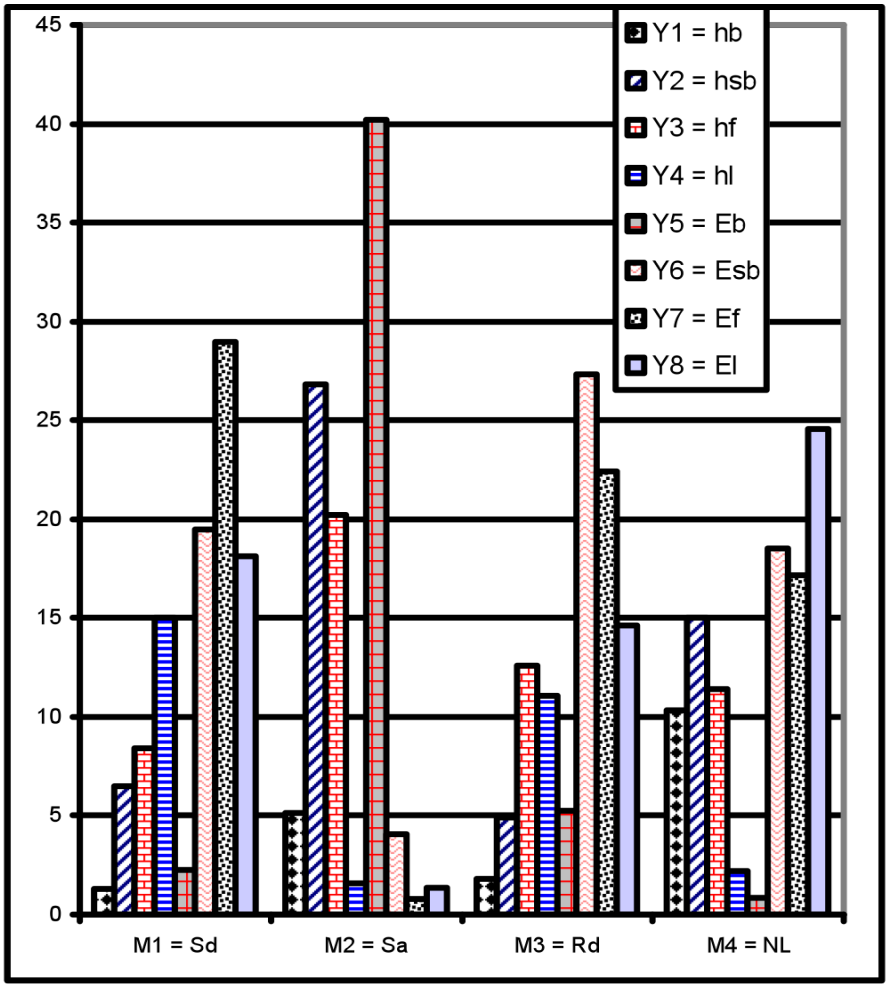

Y_1	h_b
Y_2	h_{sb}
Y_3	h_f
Y_4	h_l
Y_5	E_b
Y_6	E_{sb}
Y_7	E_f
Y_8	E_l

Fig. 16 Uncertainty propagation indicator for each control variable

14. Conclusion

The objective of this guideline is to propose a numerical method which allows accounting for the variability of the mechanical and geometrical properties of a railway track. This variability due to the heterogeneity of the subgrade or due to drainage problem is characterized from in-situ measurements achieved in the frame of Innotrack (Panda measurements for example).

The main recommendations regarding stochastic analyses are:

- To apply the stochastic finite element method (SFEM) based on a stochastic collocation procedure which allows to easily estimate the first and second order moments of the response process or any control random variable linked to this process. To study the propagation of mechanical and geometrical uncertainties through the FE model.

- To adopt the presented methodology to decrease time computation. As an example, if we consider one parameter characterized by its mean value and its standard deviation, only 4 simulations are needed to evaluate the mean and the standard deviation of the acceleration of track.